Research Square

Preprints are preliminary reports that have not undergone peer review.
They should not be considered conclusive, used to inform clinical practice,
or referenced by the media as validated information.

An ET-dependent VPD threshold frontier of cropland water–carbon coupling and its modulation by deep soil water under salinized irrigation: evidence from the Hetao Irrigation District, China

Xianzhi Wang
Qilu Normal University
Yanying Wang
20176917@qlnu.edu.cn
Qilu Normal University
kang Pian
Qilu Normal University
Xinyue Gao
Qilu Normal University

Research Article

Keywords: Hetao Irrigation District, evapotranspiration, gross primary productivity, vapor pressure deficit, threshold frontier, salinized cropland

Posted Date: April 21st, 2026

DOI: https://doi.org/10.21203/rs.3.rs-9307876/v1

License: This work is licensed under a Creative Commons Attribution 4.0 International License.
Read Full License

Additional Declarations: No competing interests reported.

[Title] An ET-dependent VPD threshold frontier of cropland water–carbon coupling and its modulation by deep soil water under salinized irrigation: evidence from the Hetao Irrigation District, China

[Author Names] Xianzhi Wang [1], Yanying Wang [1, *], Kang Pian [1], Xinyue Gao [1]

[Affiliations] [1] College of Geography and Tourism, Qilu Normal University, Jinan 250000, China

[Corresponding Author]

Corresponding author. E-mail address: 20176917@qlnu.edu.cn (Y. Wang) Tel.: +86-18053117135

Funding: This study was funded by the Natural Science Foundation of Shandong Province, China (ZR2024QD284).

Competing Interests: The authors declare that they have no known competing financial interests or personal relationships that could have appeared to influence the work reported in this paper.

CRediT Author Statement: Xianzhi Wang: Conceptualization, Methodology, Software, Writing - Original draft. Yanying Wang: Data curation, Formal analysis, Writing - Review & Editing. Kang Pian: Supervision, Resources, Visualization. Xinyue Gao: Formal analysis, Funding acquisition.

An ET-dependent VPD threshold frontier of cropland water–carbon coupling and its modulation by deep soil water under salinized irrigation: evidence from the Hetao Irrigation District, China

Abstract

Understanding when additional water consumption ceases to yield proportional carbon gain is essential for irrigation-dominated croplands exposed to strong atmospheric demand. Using the Hetao Irrigation District in arid northern China as a representative system, we developed a frontier-based framework to diagnose how evapotranspiration (ET), vapor pressure deficit (VPD), and deep soil water background jointly constrain gross primary productivity (GPP). Native 8-day PML-V2a ET and GPP estimates for 2019–2024 were combined with ERA5-Land meteorological variables on a common 1 km cropland grid. A generalized additive model was used to reconstruct the marginal effect of VPD on GPP in ET–VPD space, and the zero-isoline of that surface was extracted as the functional VPD threshold frontier. The cropland GPP–ET relationship showed clear nonlinearity and a stable main breakpoint of 12.98 mm/8d (95% CI: 12.49–13.86 mm/8d), indicating a transition from a relatively stronger water-limited stage to a stage of diminishing marginal returns. The tolerable VPD upper bound increased with ET at first, but began to contract once ET approached the breakpoint, revealing an ET-dependent dynamic frontier rather than a fixed VPD threshold. Subgroup fitting further showed that the deep soil water availability index (DSWI) mainly shifted the frontier position: the breakpoint occurred at 7.18 mm/8d under low DSWI and at 9.35 mm/8d under high DSWI, corresponding to a rightward shift of 2.17 mm/8d. Seasonal diagnostics indicated that May–July constituted a high-growth yet high-risk window, while spatial risk clustered in downstream, poorly drained, and salinity-prone parts of the district. Quantile frontiers and a cross-product robustness test using independent GOSIF GPP preserved the same nonlinear saturation pattern. These results suggest that VPD

primarily controls frontier shape whereas deep soil water background regulates system vulnerability mainly by shifting the threshold position.

Keywords: Hetao Irrigation District; evapotranspiration; gross primary productivity; vapor pressure deficit; threshold frontier; salinized cropland

1. Introduction

Water consumption and carbon assimilation are intrinsically coupled in cropland ecosystems. Evapotranspiration (ET) integrates transpiration and evaporation, whereas gross primary productivity (GPP) represents ecosystem carbon uptake; together they govern water use efficiency, productivity formation, and drought vulnerability (Allen et al., 1998; Monteith, 1965; Novick et al., 2016). In many agronomic and ecohydrological studies, the GPP–ET relationship is implicitly treated as monotonic, so larger water consumption is assumed to support proportionally larger carbon gain. However, stomatal regulation, hydraulic safety, and rising atmospheric aridity imply that such proportionality should weaken once water flux and atmospheric demand exceed a certain range (Jarvis, 1976; Oren et al., 1999; Sperry et al., 2002).

Over the last two decades, research has increasingly emphasized the role of vapor pressure deficit (VPD) in regulating terrestrial carbon and water fluxes. Stomata generally become more sensitive to VPD as atmospheric demand rises, which can suppress photosynthesis even when soil or irrigation water is still available (Katul et al., 2010; Medlyn et al., 2011; Oren et al., 1999). At broader scales, atmospheric demand has been shown to exert increasingly strong control on ecosystem conductance, transpiration, and carbon uptake (Novick et al., 2016). A large synthesis by Grossiord et al. (2020) further highlighted that rising VPD induces a cascade from stomatal closure to reduced photosynthesis and heightened hydraulic risk. Yet most existing analyses still estimate average responses of GPP to VPD or ET, rather than directly diagnosing the productivity boundary at which VPD shifts from tolerable to suppressive.

An equally important shift in the recent literature is that the question is no longer whether VPD matters, but under what conditions atmospheric dryness or soil water limitation becomes the dominant

control on ecosystem function. Global evidence shows that productivity loss under drought cannot be attributed to a single universal driver: in many regions soil moisture remains the primary determinant of whether production becomes water-limited, yet that dominance varies with ecosystem type, time scale, and background water supply (Fang and Leung, 2022; Liu et al., 2020; Novick et al., 2024). Newer China-wide evidence further suggests that the relative dominance of atmospheric and soil dryness itself shifts across identifiable threshold ranges, with croplands and semi-arid systems showing especially sensitive transitions (Wang et al., 2025). For irrigated croplands, this implies that the critical issue is not which factor is universally stronger, but when continuous water supply ceases to buffer the system and a VPD-controlled boundary begins to emerge.

For irrigated croplands, the problem is even more complex. Artificial irrigation alters water supply, shallow groundwater and deeper subsurface moisture can buffer atmospheric drought, and long-term evaporative concentration can generate salinity-prone landscapes with strong spatial heterogeneity (Ao et al., 2024; Feng et al., 2005; Yu et al., 2010). Under such conditions, discussing only a mean VPD effect or only a soil-moisture effect is insufficient. What is needed is a framework that can answer two linked questions: first, whether cropland productivity is bounded by an ET-dependent VPD frontier rather than a fixed VPD threshold; and second, whether deeper moisture background changes the shape of that frontier or mainly shifts its position.

The Hetao Irrigation District (HID) in the upper Yellow River Basin provides an appropriate natural laboratory to address these questions. HID is a typical diversion-irrigation district in an arid to semi-arid climate, where low precipitation coexists with strong atmospheric demand, dense irrigation–drainage infrastructure, shallow groundwater influence, and a long history of secondary salinization(Guo and Liu, 2021; Ramos et al., 2023). The coexistence of strong atmospheric pull, large anthropogenic water supply, and salinized environmental background makes HID especially suitable for diagnosing threshold behavior in cropland carbon–water coupling.

Recent advances in remote sensing now make such diagnosis feasible. Native 8-day PML-V2a products provide internally consistent ET and GPP estimates in a coupled water–carbon framework (He et

al., 2022; Xu et al., 2026, discussion paper under review; Y. Zhang et al., 2019), while independent GOSIF products offer both SIF and SIF-derived GPP data for robustness testing (Li et al., 2025; Li and Xiao, 2019). ERA5-Land provides meteorological forcing and deep-layer soil moisture with continuous spatiotemporal coverage (Muñoz-Sabater et al., 2021). Together with generalized additive modelling, quantile-based robustness checks, and frontier extraction, these datasets permit a boundary-oriented rather than mean-oriented diagnosis of cropland vulnerability (Koenker, 2005; Wood, 2017).

Moreover, prior work has already shown that ET and VPD are not linked through a simple monotonic relation, but can display clear nonlinearity and hysteresis; similarly, the coupling among GPP, ET, and VPD can bend or saturate once water consumption and atmospheric demand reach high levels (Zhang et al., 2014, 2019). What remains comparatively rare is to translate that structure into a functional upper boundary that can be explicitly extracted and interpreted. In ecology, quantile regression and upper-envelope thinking have long been used to identify limiting boundaries rather than average tendencies (Cade and Noon, 2003). Accordingly, the combination of GAM-based derivatives, frontier extraction, and quantile robustness adopted here is valuable not only because it is flexible, but because it converts a fitted response surface into an ecologically interpretable tolerable limit.

Against this background, the objectives of this study are to determine (1) whether the cropland GPP–ET relationship in HID exhibits a stable nonlinear breakpoint and a stage of diminishing marginal returns; (2) whether the tolerable upper limit of VPD forms an ET-dependent dynamic frontier; and (3) whether deep soil water background mainly changes frontier shape or shifts frontier position. We hypothesize that VPD controls the shape of the productivity boundary, whereas deeper soil moisture background primarily regulates system vulnerability by moving the threshold laterally rather than by redefining the boundary itself.

2. Data and methods

2.1 Study area

As shown in Figure 1, the Hetao Irrigation District is located along the upper Yellow River in western Inner Mongolia, China, and is one of the largest diversion-irrigation districts in the country. Cropland is spatially continuous, terrain is generally flat, and agricultural production is tightly controlled by a hierarchical irrigation–drainage network. The climate is arid to semi-arid, with low precipitation but strong evaporative demand. The main crops are wheat, maize, and sunflower, and the effective growing season usually extends from April to October.

In this study, salinization is treated as an environmental setting rather than as a direct explanatory variable in the core frontier model. This choice is deliberate. Our primary objective is to diagnose the ET-dependent VPD boundary itself and then evaluate how deeper moisture background modifies the position of that boundary. In HID, long-term irrigation, fluctuating shallow groundwater, evaporative concentration, and uneven drainage jointly generate a salinized landscape (Ao et al., 2024; Feng et al., 2005; Yu et al., 2010). Therefore, the salinized background is expressed through the study-area context, the spatial risk pattern, and the interpretation of frontier vulnerability rather than through a single salinity term in the main model.

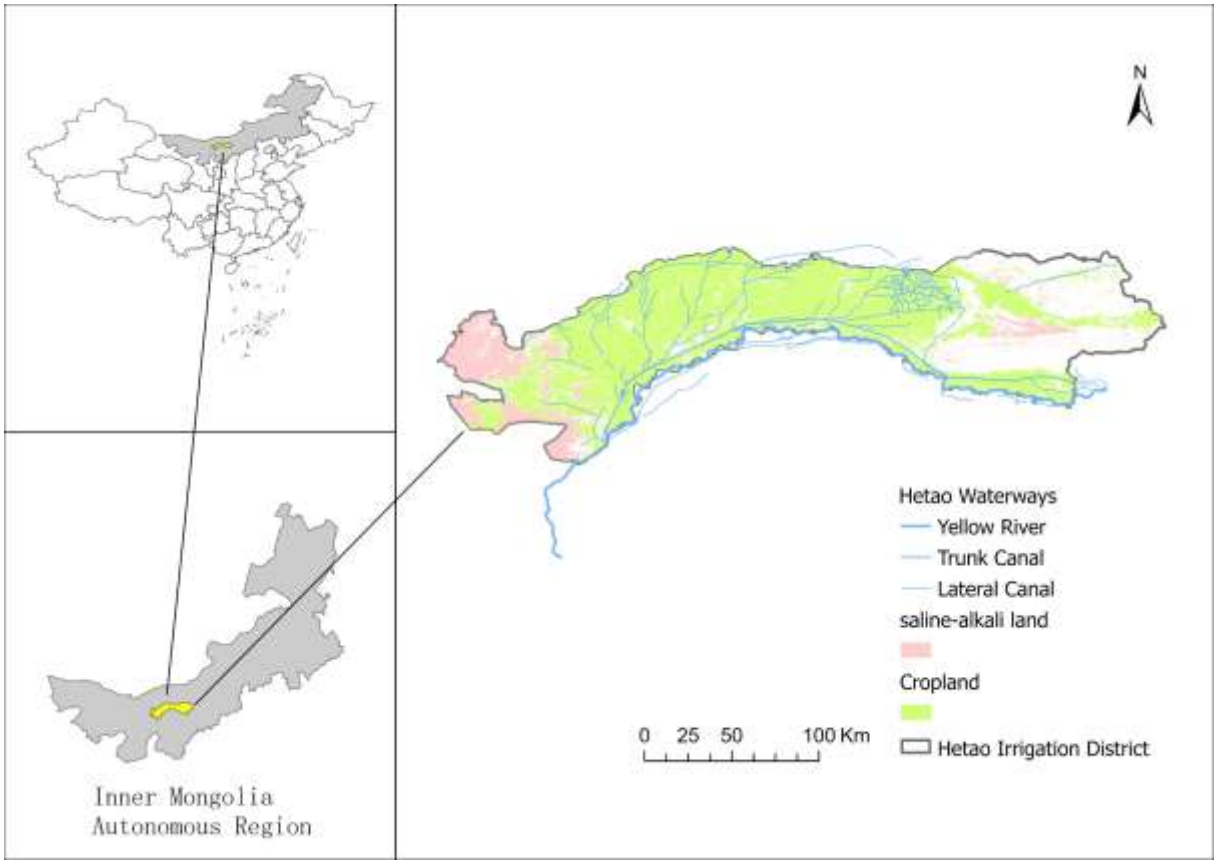


Figure 1. Location of the Hetao Irrigation District, cropland distribution, salinized background and irrigation–drainage system overview.

2.2 Data sources and preprocessing

The core panel was constructed from native 8-day PML-V2a products for 2019–2024. PML-V2a provides internally coupled ET and GPP estimates at 500 m resolution based on a water–carbon framework (He et al., 2022; Xu et al., 2026, discussion paper under review; Q. Zhang et al., 2019). We used the native 8-day product directly rather than disaggregating monthly values, because the purpose of this study is to diagnose short-term frontier behavior under concurrent water flux and atmospheric demand.

Meteorological variables were obtained from ERA5-Land, including air temperature, dew-point temperature, precipitation, and volumetric soil water content in the fourth layer (100–289 cm) (Muñoz-Sabater et al., 2021). These variables were aggregated to the same 8-day steps and extracted to a common 1 km cropland grid skeleton. Continuous variables were harmonized using bilinear interpolation, whereas

cropland masks were resampled using nearest-neighbor assignment. Sample screening retained only pixels with cropland fraction ≥ 0.5, records within the April–October growing season, and samples above the 20th percentile of GPP to exclude off-season and near-bare-soil states. Throughout the manuscript, remote-sensing and reanalysis variables are treated as gridded products or estimates rather than as direct field observations.

Figure 2 summarizes the spatial pattern of the main variables used in the analysis. ET and GPP display clear cropland-dependent gradients, while VPD and deep soil water show strong west–east and local hydrological contrasts. These heterogeneous but physically coherent gradients provide the empirical basis for identifying whether the productivity boundary shifts under different atmospheric and subsurface conditions.

Dataset	Main variables	Resolution	Temporal scale	Role in this study
PML-V2a	Native 8-day ET and GPP	500 m	8-day	Main ET and GPP source; harmonized to the 1 km cropland grid
ERA5-Land	Air temperature, dew-point temperature, precipitation, deep-layer soil moisture	≈0.1°	Hourly/monthly → 8-day	Meteorological forcing and DSWI proxy
Cropland mask	Cropland fraction / land use	1 km	Static mask	Cropland fraction ≥ 0.5 retained
GOSIF-GPP	Independent GPP proxy for robustness	0.05°	8-day	Cross-product robustness test only

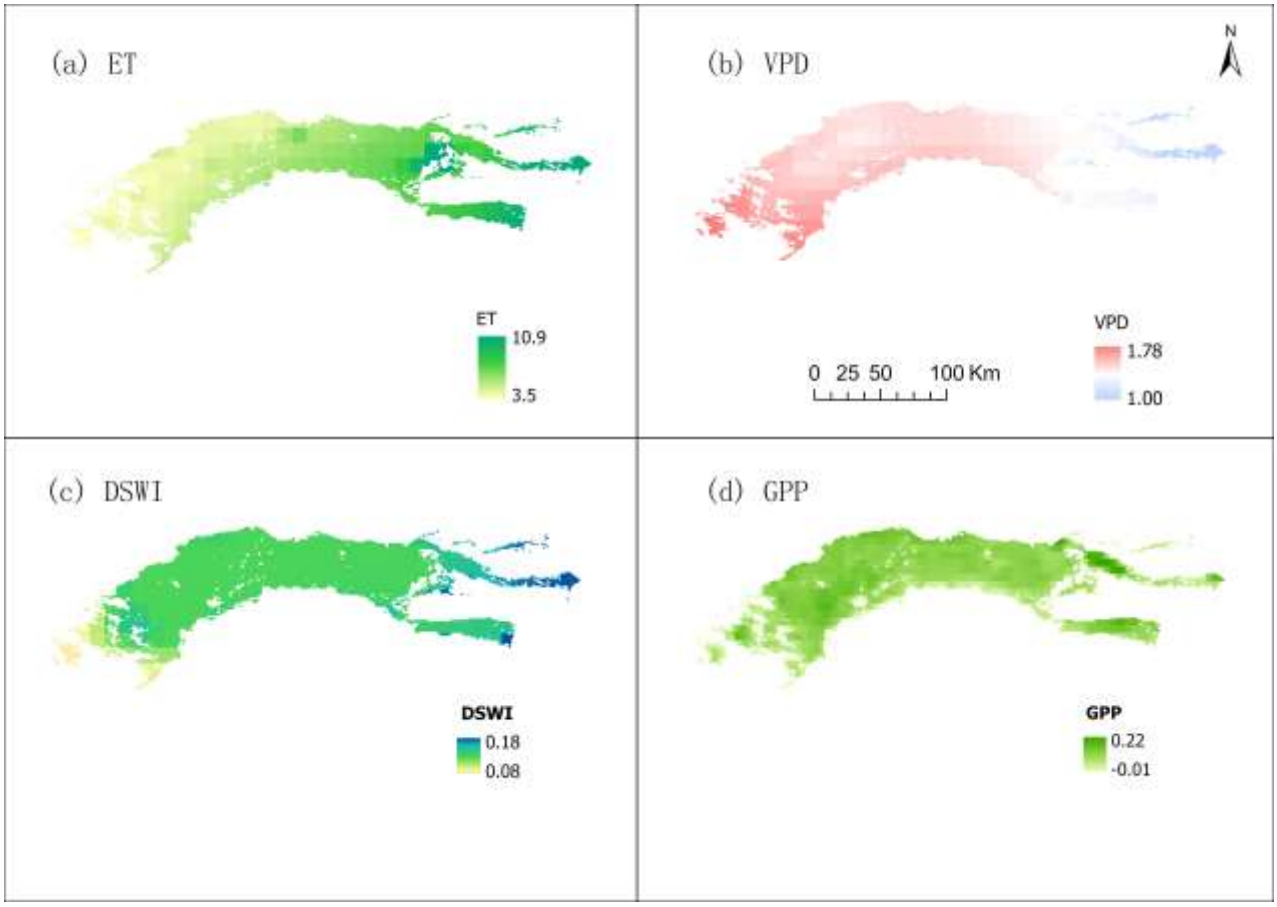


Figure 2. Spatial pattern of key variables used in the frontier analysis, including ET, VPD, DSWI and GPP.

2.3 Variable definitions

ET_main denotes 8-day cumulative evapotranspiration (mm/8d), and GPP_main denotes 8-day cumulative gross primary productivity (gC m^{-2} $8d^{-1}$). Vapor pressure deficit (VPD, kPa) was computed from 8-day mean air temperature T and dew-point temperature T_d following the FAO-56 formulation (Allen et al., 1998):

$$e_s(T) = 0.6108 \cdot exp\left(17.27T/(T + 237.3)\right) \quad (1)$$

$$e_a(T_d) = 0.6108 \cdot exp\left(17.27T_d/(T_d + 237.3)\right) \quad (2)$$

$$VPD = e_s(T) - e_a(T_d) \quad (3)$$

where e_s is the saturation vapor pressure at air temperature T, and e_a is the actual vapor pressure derived from dew-point temperature T_d; both are expressed in kPa. T and T_d are expressed in °C, so VPD is also

expressed in kPa. The deep soil water availability index (DSWI) was derived from the fourth ERA5-Land soil layer and was used as a relative proxy for subsurface moisture background rather than as a calibrated estimate of groundwater depth. For the subgroup comparison, each cropland grid cell was assigned its study-period mean DSWI (2019–2024), and the median of this distribution was used to define the high-DSWI group (≥ median) and the low-DSWI group (< median). We used the study-period mean rather than year-specific dynamic grouping to preserve a stable classification of deep subsurface moisture background and to avoid confounding subgroup comparisons with interannual shifts in wetness rank.

$$VPD_{excess_i} = VPD_{obs}, i - VPD_t hr, i(ET) \quad (4)$$

$$EF = (1/n) \cdot \Sigma I(VPD_{obs}, i > VPD_{thr}, i) \quad (5)$$

Here VPD_{excess} measures the exceedance magnitude of observed VPD relative to the ET-conditioned threshold frontier; when $VPD_{excess} > 0$, the corresponding sample operates above the diagnosed frontier. EF quantifies how frequently the threshold is exceeded over a given period and is therefore used to characterize cumulative exposure to frontier-related risk in both seasonal and spatial analyses. The DSWI comparison is interpreted as a contrast between wetter and drier deep subsurface backgrounds. It is designed to test whether the ET-dependent VPD threshold frontier shifts consistently under contrasting subsurface conditions, rather than to numerically infer groundwater depth.

2.4 Frontier identification and robustness analysis

To characterize the nonlinear $GPP - ET - VPD$ relationship, we fitted a generalized additive model (GAM) in R using the mgcv package (Wood, 2017). Penalized regression splines were used for the univariate smooth terms, and a tensor-product smooth was used for the $ET \times VPD$ interaction. Smoothing parameters and effective degrees of freedom were selected automatically by restricted maximum likelihood (REML). Using 1,737,842 screened 8-day cropland samples, the final GAM achieved an adjusted R^2 of 0.917, an RMSE of 6.73 g C m^{-2} $8d^{-1}$, and a highly significant overall fit ($F = 402{,}849.3$, $p < 0.001$). Model adequacy was further evaluated by inspection of residual patterns and significance tests for the smooth terms.

$$GPP = s1(ET) + s2(VPD) + ti(ET, VPD) + \varepsilon \quad (6)$$

where $s1(ET)$ and $s2(VPD)$ are univariate smooth functions, $ti(ET, VPD)$ is the tensor-product interaction term describing the joint nonlinear response surface, and ε is the residual error. We used $Eq.(6)$ to reconstruct how the marginal effect of VPD on GPP changes across ET states, and we extracted the zero-isoline of $\partial GPP/\partial VPD$ as the ET-dependent VPD threshold frontier. The ET–VPD support domain used for this diagnosis is shown in Supplementary Figure S2.

The model was used for diagnosis rather than simple prediction. Physiologically, the extracted boundary is intended to represent the upper VPD condition under which cropland carbon uptake can still be maintained without an additional net penalty from atmospheric drying. Once the marginal effect of VPD becomes negative, the system is interpreted as moving from a tolerable operating range toward a suppressive range in which stomatal regulation and hydraulic protection increasingly constrain photosynthesis (Novick et al., 2024; Oren et al., 1999; Sperry et al., 2002).

The extracted frontier points were then fitted with a piecewise linear regression to estimate the main ecohydrological breakpoint. Uncertainty was quantified using 500 paired bootstrap resamples of the extracted frontier points with replacement. Because sparse support near the tails can destabilize the frontier, subgroup and quantile frontiers were interpreted only within robust ET support regions. The ET–DSWI support structure used to evaluate subgroup support is shown in Supplementary Figure S3. The low- and high-DSWI subgroup breakpoints were therefore used to diagnose relative lateral displacement rather than absolute one-to-one numerical comparability with the full-sample breakpoint.

To assess robustness beyond mean fitting, we additionally derived quantile generalized additive model (QGAM) frontiers for the median, 75th percentile, and 90th percentile conditions, following the logic of quantile regression (Koenker, 2005). If the turning point remains concentrated within a narrow ET range across these alternative frontiers, the breakpoint can be regarded as structurally stable rather than as an artifact of a single fitting strategy.

Finally, to test whether the detected nonlinear pattern might simply reflect shared structure within one coupled product framework, we replaced PML-derived GPP with the independent GOSIF-derived GPP product while keeping PML ET unchanged. From a reproducibility perspective, the key inferential target is the stability of the sign-change boundary rather than the exact tail behavior of any single fitted curve.

Table 1 summarizes the final threshold metrics used consistently throughout the manuscript.

Metric	Value	Interpretation
Main ecohydrological breakpoint	12.98 mm/8d	95% CI: 12.49–13.86
Low DSWI breakpoint	7.18 mm/8d	Subgroup frontier
High DSWI breakpoint	9.35 mm/8d	Subgroup frontier
Threshold shift	+2.17 mm/8d	High DSWI relative to low DSWI
QGAM median frontier	13.40 mm/8d	Robustness check
QGAM 75th percentile frontier	13.86 mm/8d	Robustness check
QGAM 90th percentile frontier	12.49 mm/8d	Robustness check

3. Results

3.1 The cropland GPP–ET relationship shows strong nonlinearity and diminishing marginal returns

Using the native 8-day PML panel, the scatter structure of GPP against ET shows that carbon assimilation in the Hetao cropland system does not increase linearly with water consumption (Xu et al., 2026). Instead, GPP rises rapidly at low ET and then enters a clear stage of diminishing marginal returns (Figure 3). This means that additional water consumption under irrigation does not necessarily deliver

equivalent additional carbon gain, and the efficiency of water use weakens once ET exceeds a moderate range.

Piecewise fitting indicates that this transition has a stable quantitative expression. The main ecohydrological breakpoint identified from the full sample is 12.98 mm/8d, with a 95% confidence interval of 12.49–13.86 mm/8d. When 8-day cumulative ET approaches this level, the marginal gain of GPP per unit ET declines sharply. The breakpoint should therefore be interpreted as a regional turning point in carbon–water coupling efficiency rather than as a fixed physiological constant for an individual crop or growth stage.

The geometry of the scatter cloud adds process meaning to this pattern. At low ET, observations are widely dispersed, implying strong co-control by crop condition, irrigation timing, and atmospheric background. As ET increases, observations become increasingly bounded by an upper envelope. In other words, the system progressively shifts from supply-dominated behavior to boundary-dominated behavior, which directly motivates the frontier analysis below.

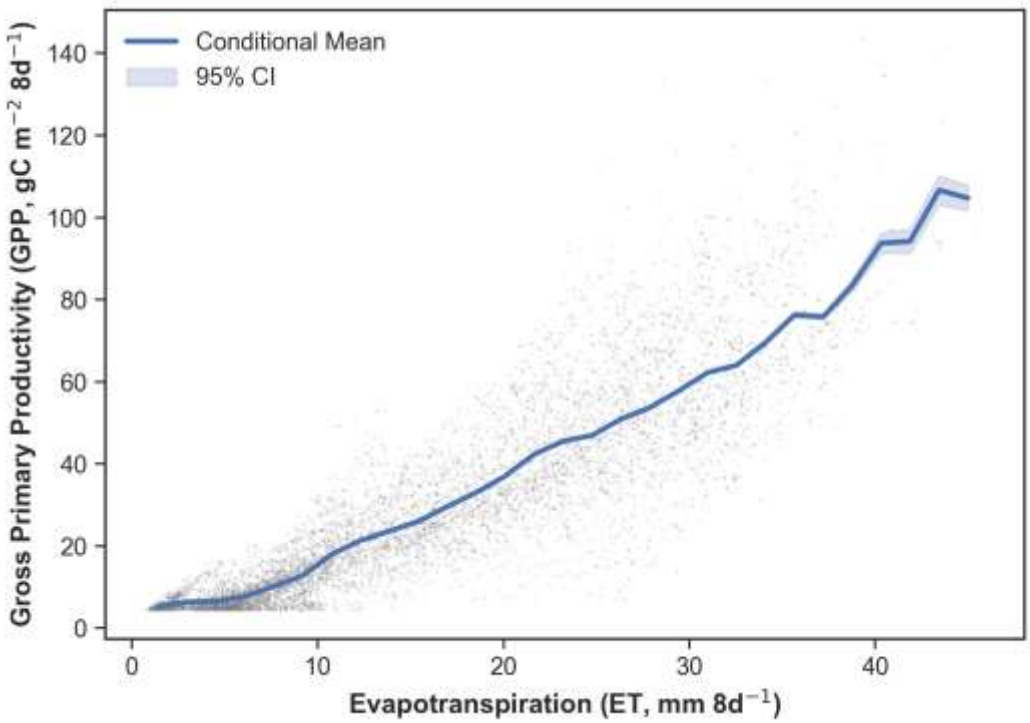


Figure 3. Nonlinear GPP–ET relationship and the onset of diminishing marginal returns

3.2 VPD shapes an ET-dependent dynamic frontier of cropland productivity

The two-dimensional ET–VPD response surface demonstrates that the effect of atmospheric dryness on productivity depends strongly on ET state (Figure 4). Under low ET, increasing VPD generally exerts a strong negative marginal effect on GPP, indicating that when water flux is already limited, higher atmospheric demand is rapidly translated into reduced carbon assimilation. Under moderate ET, the negative effect of VPD weakens, revealing stronger resistance to atmospheric dryness when the system maintains a larger water flux.

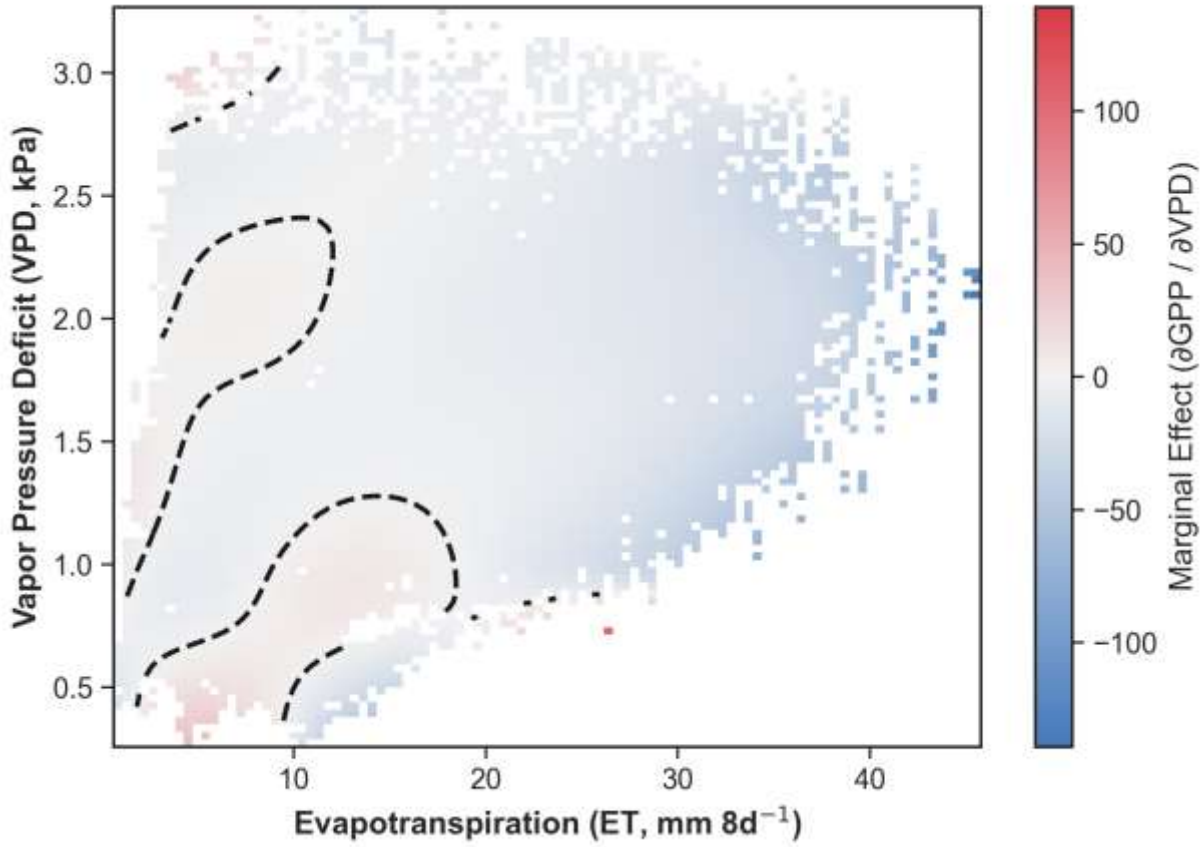


Figure 4. Marginal effect of VPD on GPP in ET–VPD space

The frontier extracted from the zero-isoline of ∂GPP/∂VPD reveals a typical ET-dependent threshold structure (Figure 5). The tolerable upper bound of VPD increases with ET at first, but once ET approaches

the main breakpoint, the upper bound ceases to expand and starts to contract. This demonstrates that the system does not operate under a single fixed VPD threshold. Rather, the effective VPD limit is conditional on water-flux status and becomes dynamic in ET space. In this sense, the frontier is best understood as a functional upper boundary of tolerable atmospheric dryness, not as the earliest detectable signal of physiological stress.

Importantly, the detected breakpoint of 12.98 mm/8d should be interpreted in a restrained way. When 8-day cumulative ET approaches this level, the marginal gain of GPP from additional ET declines markedly, suggesting that the system shifts from a relatively stronger water-limited stage to a stage of diminishing marginal returns. Additional water consumption beyond this level may therefore fail to produce proportional gains in carbon assimilation.

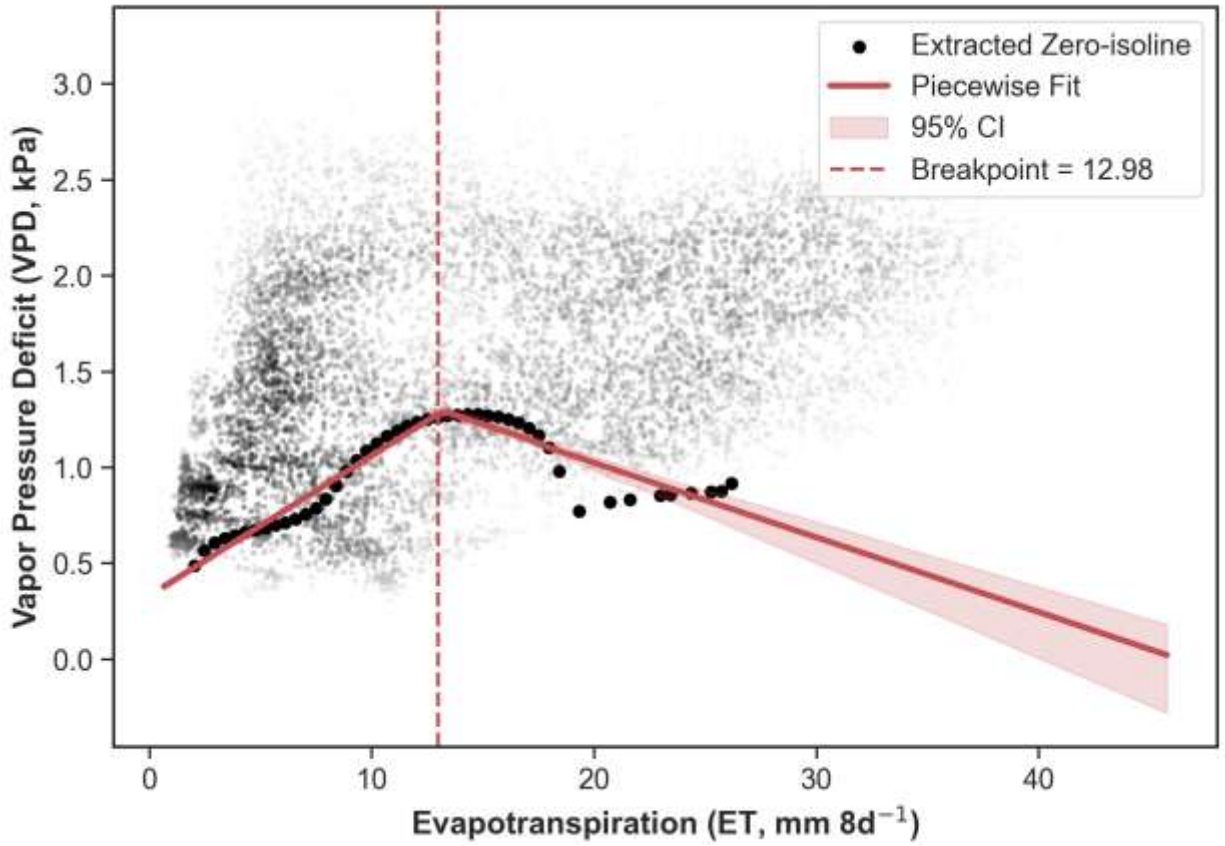


Figure 5. ET-dependent VPD frontier and piecewise fit

3.3 Deep soil water background primarily shifts the frontier position

Subgroup analysis shows that deep soil water background does not create a new frontier form but significantly shifts the position at which the system enters the diminishing-returns regime (Figure 6; Supplementary Figure S3). Under low DSWI conditions, the identified breakpoint is 7.18 mm/8d; under high DSWI conditions, it moves rightward to 9.35 mm/8d, corresponding to a shift of +2.17 mm/8d. This indicates that deeper moisture background allows the system to sustain higher ET before entering a stress-controlled state.

The interpretation of these subgroup frontiers requires care. The low- and high-DSWI curves are extracted from conditional subsamples, so their breakpoint values are not intended for absolute one-to-one comparison with the full-sample breakpoint of 12.98 mm/8d. More fundamentally, the subgroup fits are estimated within different ET support domains and with different sample compositions, so their absolute breakpoints are not numerically commensurate with the full-sample value. Their primary role is to identify the relative shift in threshold position under contrasting subsurface moisture backgrounds. Accordingly, the most informative quantity in Figure 6 is the direction and magnitude of the lateral shift, rather than the exact trajectory of the tails.

Process-wise, the result suggests that deep soil water acts mainly as a buffering background. Under lower DSWI, the system reaches its threshold earlier, indicating that stomatal defense and reduced carbon gain emerge under smaller water fluxes. Under higher DSWI, this transition is delayed, meaning that the frontier is displaced toward larger ET values while the basic boundary framework remains intact.

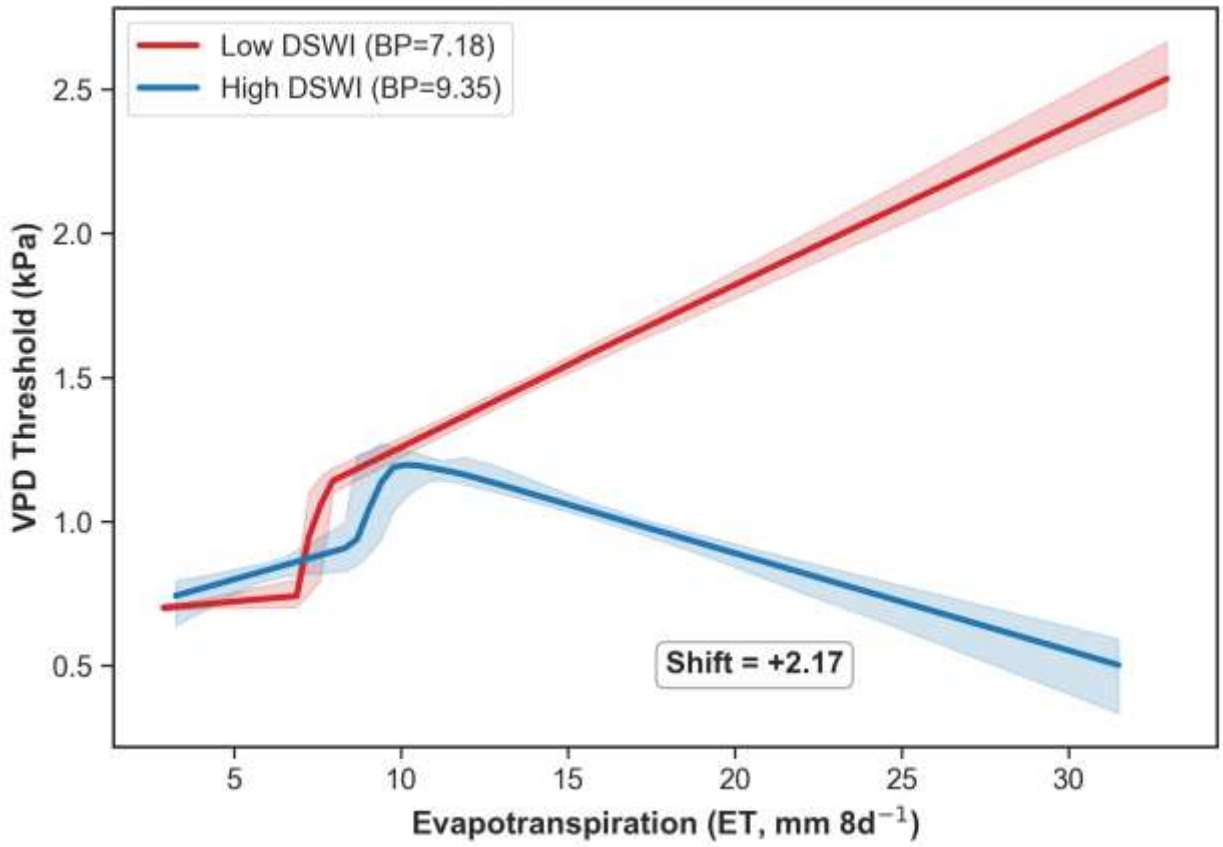


Figure 6. DSWI-induced lateral shift of the threshold frontier

3.4 Seasonal and spatial diagnostics reveal a concentrated risk window

Monthly diagnostics (Supplementary Figure S1) show that frontier exceedance is not evenly distributed across the growing season. ET and GPP both rise rapidly from spring to summer, but the increase in productivity coincides with a stronger probability of operating near or above the VPD threshold. The main risk window occurs from May to July, when water consumption and carbon gain are both high but atmospheric demand is sufficiently strong to push a large fraction of observations toward the suppressive side of the frontier. By late season, the risk weakens as VPD declines and the system retreats toward or below the threshold.

Spatially, frontier-related risk is strongly heterogeneous (Figure 7). High-risk zones tend to cluster in downstream, poorly drained, and salinity-prone parts of the irrigation district. This pattern is consistent with

the study-area context, in which irrigation–drainage imbalance, shallow groundwater influence, and secondary salinization co-occur in specific spatial units. Thus, the frontier should be understood not only as a regional average threshold, but also as a diagnostic tool for identifying spatially vulnerable cropland clusters within the irrigation district.

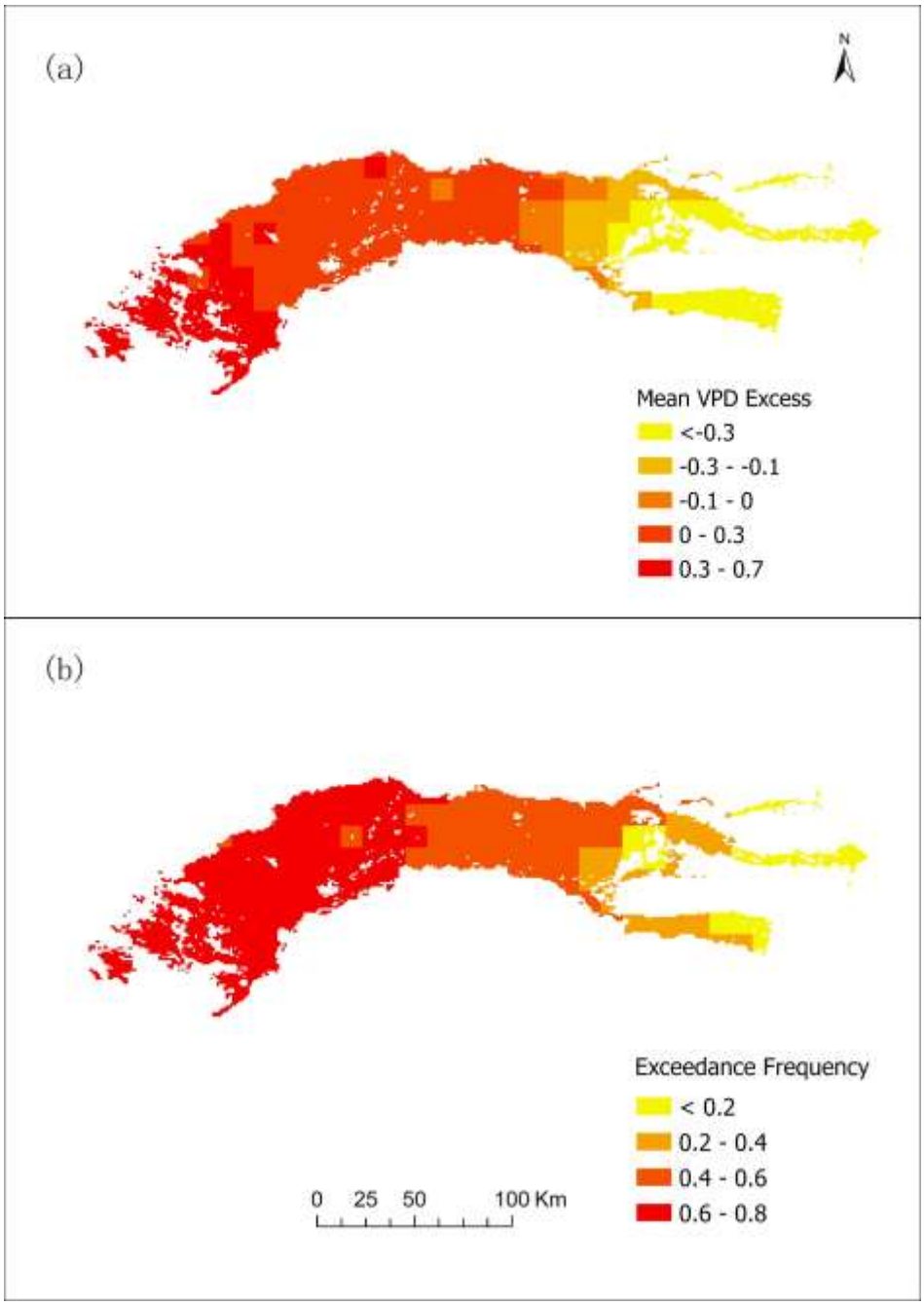


Figure 7. Spatial risk diagnostics of mean VPD excess and exceedance frequency

3.5 Quantile and cross-product tests confirm that the frontier is robust

To evaluate whether the detected boundary merely reflects mean fitting, QGAM frontiers were estimated for the median, 75th percentile, and 90th percentile conditions (Figure 8). The corresponding breakpoints are approximately 13.40, 13.86, and 12.49 mm/8d, respectively. Although the local shape of the frontier varies slightly across quantiles, all turning points remain concentrated within a narrow range around the main breakpoint. This convergence indicates that the ecohydrological turning point is structurally stable rather than a by-product of a single fitting strategy.

A second robustness test replaced PML GPP with the independent GOSIF-derived GPP product while retaining PML ET. The nonlinear saturation of the GPP–ET relationship remained clearly visible. Therefore, the observed frontier is unlikely to be an artifact of shared assumptions within a single ET–GPP product framework. Instead, it reflects a genuine ecohydrological signal in the Hetao cropland system.

Taken together, the full-sample frontier, the DSWI subgroup comparison, the quantile frontiers, and the cross-product substitution all point to the same conclusion: HID croplands exhibit a stable ET-dependent VPD threshold frontier, and deep soil water background mainly regulates vulnerability by shifting the threshold position rather than by redefining the existence of the frontier.

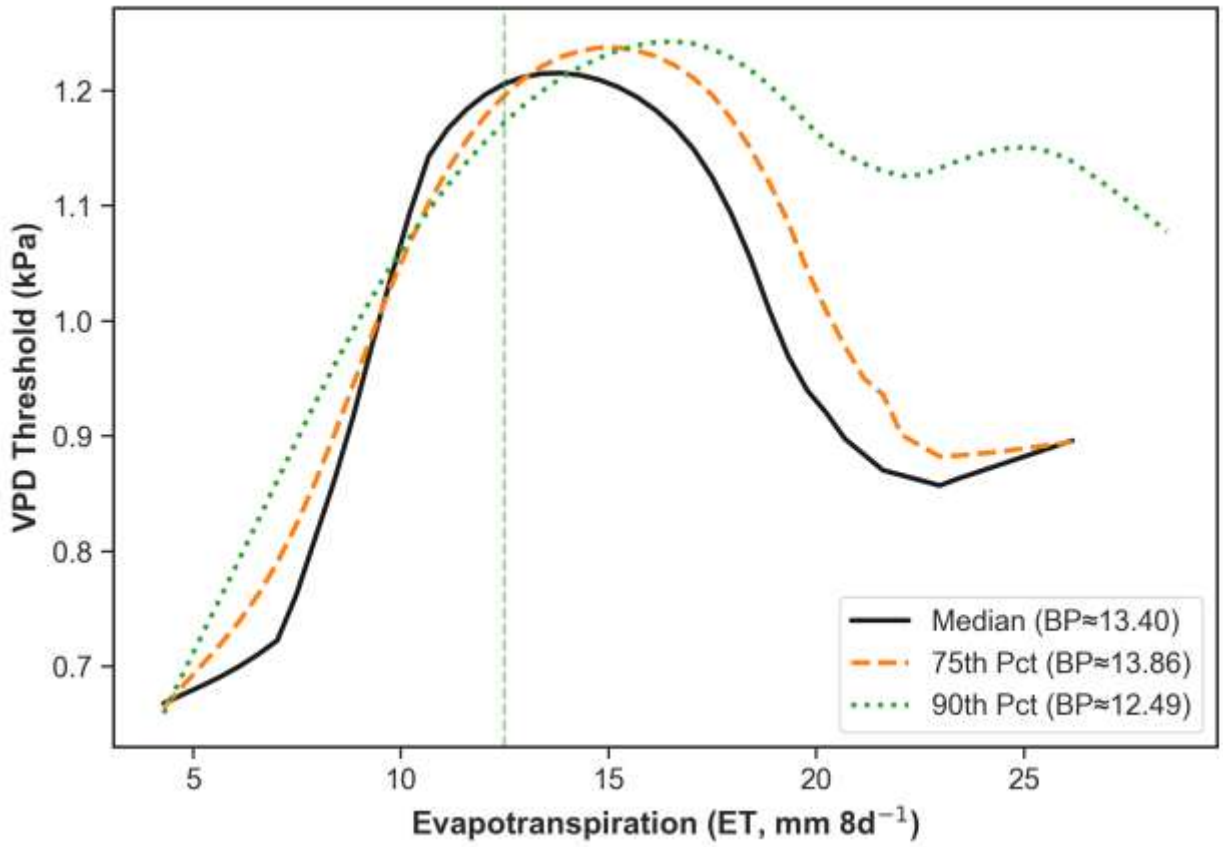


Figure 8. Quantile-frontier robustness of the ecohydrological breakpoint

4. Discussion

4.1 From mean response to boundary diagnosis

A major contribution of this study is the shift from average-response analysis to boundary diagnosis. Many previous studies have evaluated the mean sensitivity of GPP, ET, or water use efficiency to VPD and soil moisture (Novick et al., 2016; Zhou et al., 2014). Such analyses are important, but they do not directly answer when the system begins to experience a net suppressive effect of atmospheric demand under a given water-flux state. By extracting the zero-isoline of ∂GPP/∂VPD, our approach identifies a functional upper boundary in ET–VPD space and therefore separates the notion of 'average effect' from that of 'operating limit'.

This distinction matters in irrigated croplands. In HID, irrigation can maintain relatively high ET even under strong atmospheric demand. If only mean effects were considered, one might conclude either that VPD is universally suppressive or that irrigation fully neutralizes atmospheric stress. The frontier perspective reveals a more nuanced pattern: increasing ET enhances tolerance to VPD only up to a point, after which the safe operating boundary contracts. Unlike leaf- or plot-scale threshold definitions based on a 50% decline in stomatal conductance, abrupt reductions in assimilation, or critical hydraulic points, the frontier used here is an emergent system-scale boundary estimated from gridded products. It does not mark the first onset of strain; rather, it marks the point beyond which additional atmospheric drying is associated with a net negative marginal effect on GPP under a given ET state. This scale distinction is important because irrigation management operates at field-to-district scale, where the practical question is not when crops first sense stress, but when continued water consumption no longer offsets atmospheric demand efficiently.

4.2 Why deep soil water mainly appears as a lateral shift

The subgroup results indicate that DSWI primarily shifts the breakpoint position rather than reconstructing the frontier shape. This interpretation is consistent with the ecohydrological role of deeper subsurface moisture. At short time scales, stomata respond directly to atmospheric demand and leaf-to-root hydraulic status, but the background availability of deeper water determines how long a crop can sustain exchange before defensive regulation is triggered (Oren et al., 1999; Sperry et al., 2002). In that sense, VPD determines the geometry of the boundary, whereas deeper moisture background determines where along the ET axis the system begins to experience that boundary.

This finding also helps reconcile two apparently conflicting views in the literature. Some studies emphasize atmospheric demand as the dominant regulator of water and carbon fluxes, whereas others emphasize the primacy of soil water supply (Grossiord et al., 2020; Novick et al., 2016). Our results suggest that these are not mutually exclusive. In HID croplands, atmospheric demand controls the frontier itself, but deeper water availability alters the location at which the frontier becomes active. The DSWI

effect is therefore better understood as a vulnerability modulation term than as a first-order replacement for VPD control.

Seen in this way, disagreement across previous studies does not necessarily imply contradiction; rather, different studies may be identifying different layers of water limitation. When the system is primarily constrained by insufficient soil supply, soil moisture is more likely to determine whether production enters a stressed state; when irrigation or deeper water background sustains relatively high ET, VPD is more likely to appear as the controlling upper-bound term (Fang et al., 2021; Liu et al., 2020; Novick et al., 2024; Wang et al., 2025). Our formulation that 'VPD shapes the frontier, whereas deeper moisture background shifts its position' should therefore be read as a redistribution of control across constraint levels, not as a rejection of the broader VPD-versus-soil-moisture literature.

4.3 Seasonal and spatial implications under a salinized background

The seasonal analysis shows that the frontier has immediate agronomic meaning. The highest productivity phase is also the period in which the system most frequently approaches or exceeds the VPD threshold. This means that management based solely on seasonal averages may underestimate the risk concentration in late spring and early summer. A threshold framework can therefore complement irrigation scheduling by identifying not only when water demand is high, but when additional water use is no longer translated efficiently into carbon gain.

Spatially, the clustering of risk in downstream, poorly drained, and salinity-prone sectors indicates that the frontier is embedded in the broader water–salt landscape of HID. This is important because the manuscript does not claim that soil salinity was explicitly estimated as a dynamic driver in the core statistical model. Instead, salinity is treated as a regional background condition, and the spatial concentration of threshold exceedance in salinity-prone areas provides process-consistent evidence that carbon–water vulnerability is amplified where irrigation, drainage limitation, shallow groundwater, and evaporative concentration converge (Ao et al., 2024; Feng et al., 2005; Yu et al., 2010). A plausible mechanism is that salinity adds osmotic stress and ion-related constraints on root water uptake, thereby

lowering effective water availability, leaf water potential, and hydraulic conductance (Munns and Tester, 2008), which makes the same atmospheric demand more likely to push cropland above the frontier.

This interpretation is also consistent with recent HID studies that documented pronounced spatial heterogeneity of soil salinity at canal scale and strong irrigation–drainage control on water–salt redistribution, especially in downstream units and cropland–wasteland mosaics (Ao et al., 2024; Hu et al., 2023).

4.4 Uncertainties and scope of inference

Several uncertainties should be acknowledged. First, DSWI is derived from deep-layer ERA5-Land soil moisture and is interpreted as a proxy of relative subsurface moisture background rather than as observed groundwater depth. The subgroup results should therefore be understood as comparative evidence of background buffering, not as precise groundwater diagnostics. Future work should pair this frontier framework with in situ groundwater-depth records and salinity surveys to determine where the proxy–background relation is strongest or weakest. Second, the study is conducted at regional 8-day scale and does not separate crop species or phenological stages; the identified breakpoint is thus a system-level turning point rather than a fixed physiological threshold for any single crop.

Third, ET and GPP in the main analysis are obtained from the same PML framework, which could raise concerns about shared model structure. This is why the independent GOSIF-based robustness test is essential: because the nonlinear saturation persists after product substitution, the main frontier is unlikely to be a mere algorithmic artifact. Fourth, we used a static cropland mask for the full study period, which does not capture minor interannual changes in cropland distribution at the irrigation-district margins; however, the core cropland pattern of HID remained stable during 2019–2024, so this simplification is unlikely to alter the main conclusions. Finally, the frontier should not be interpreted as a deterministic irrigation prescription. Its main value lies in diagnosing when and where marginal carbon gains decline under concurrent atmospheric demand, thereby providing an operationally meaningful but still probabilistic indicator of cropland vulnerability.

5. Conclusions

This study demonstrates that cropland water–carbon coupling in the Hetao Irrigation District is organized by an ET-dependent VPD threshold frontier rather than by a single fixed atmospheric threshold. Native 8-day PML products reveal a stable ecohydrological breakpoint at 12.98 mm/8d, beyond which the marginal carbon gain from additional water consumption declines markedly and the system enters a clear regime of diminishing returns.

The extracted frontier shows that the tolerable upper limit of VPD initially expands with ET but contracts after the breakpoint is reached, indicating that atmospheric dryness acts not as a static stress metric but as a dynamic boundary-control term on cropland productivity. Deep soil water background does not eliminate or redefine this frontier; instead, it primarily shifts the breakpoint position. Under lower DSWI, the transition into VPD suppression occurs earlier, whereas under higher DSWI it is delayed by about 2.17 mm/8d, implying that subsurface moisture background modifies when the frontier becomes active rather than whether the frontier exists. Accordingly, the diagnosed frontier is best interpreted as a functional upper bound of tolerable atmospheric dryness at irrigation-district scale rather than as the first onset of crop stress at leaf or plot scale.

Seasonal diagnostics indicate that the main vulnerability window is concentrated in the high-growth months, while spatial diagnostics reveal clear clustering of risk in downstream, poorly drained, and salinity-prone areas. Quantile and cross-product robustness tests both support the persistence of this threshold structure. Overall, the results support a parsimonious interpretation: VPD controls the frontier shape, whereas deep soil water controls the frontier position, and frontier exceedance offers a practical way to diagnose vulnerable states in salinized irrigated croplands.

Importantly, the broader relevance of this study does not lie in exporting a single numerical breakpoint to all irrigated regions, but in providing a transferable diagnostic logic. Under global warming and intensifying atmospheric dryness, irrigation systems need to evaluate not only mean water-use efficiency or mean VPD sensitivity, but also when the productivity frontier itself becomes re-constrained by atmospheric

demand under different ET states. For irrigated drylands in Central Asia, North Africa, the western United States, and other salinity-prone or shallow-groundwater-influenced agroecosystems, the proposed frontier framework offers a comparable way to identify critical risk windows, diagnose latent vulnerability, and support climate-resilient water management. In other words, the breakpoint value is region-specific, whereas the frontier-based analytical framework is potentially generalizable across water-limited irrigated landscapes.

References

Allen, R.G., Pereira, L.S., Raes, D., Smith, M., 1998. Crop evapotranspiration: Guidelines for computing crop water requirements. FAO Irrigation and Drainage Paper 56. Food and Agriculture Organization of the United Nations, Rome.

Ao, C., Jiang, D., Bailey, R.T., Dong, J., Zeng, W., Huang, J., 2024. Water, Salt, and Ion Transport and Its Response to Water-Saving Irrigation in the Hetao Irrigation District Based on the SWAT-Salt Model. Agronomy 14, 953. https://doi.org/10.3390/agronomy14050953

Cade, B.S., Noon, B.R., 2003. A gentle introduction to quantile regression for ecologists. Frontiers in Ecology and the Environment 1, 412–420. https://doi.org/10.1890/1540-9295(2003)001%5B0412:AGITQR%5D2.0.CO;2

Fang, Y., Leung, L.R., 2022. Relative Controls of Vapor Pressure Deficit and Soil Water Stress on Canopy Conductance in Global Simulations by an Earth System Model. Earth's Future 10, e2022EF002810. https://doi.org/https://doi.org/10.1029/2022EF002810

Fang, Y., Leung, L.R., Wolfe, B.T., Detto, M., Knox, R.G., McDowell, N.G., Grossiord, C., Xu, C., Christoffersen, B.O., Gentine, P., Koven, C.D., Chambers, J.Q., 2021. Disentangling the Effects of Vapor Pressure Deficit and Soil Water Availability on Canopy Conductance in a Seasonal Tropical Forest During the 2015 El Niño Drought. JGR Atmospheres 126, e2021JD035004. https://doi.org/10.1029/2021JD035004

Feng, Z.-Z., Wang, X.-K., Feng, Z.-W., 2005. Soil N and salinity leaching after the autumn irrigation and its impact on groundwater in Hetao Irrigation District, China. Agricultural Water Management 71, 131–143. https://doi.org/10.1016/j.agwat.2004.07.001

Grossiord, C., Buckley, T.N., Cernusak, L.A., Novick, K.A., Poulter, B., Siegwolf, R.T.W., Sperry, J.S., McDowell, N.G., 2020. Plant responses to rising vapor pressure deficit. New Phytologist 226, 1550–1566. https://doi.org/10.1111/nph.16485

Guo, K., Liu, X., 2021. Reclamation effect of freezing saline water irrigation on heavy saline-alkali soil in the Hetao Irrigation District of North China. CATENA 204, 105420. https://doi.org/10.1016/j.catena.2021.105420

He, S., Zhang, Y., Ma, N., Tian, J., Kong, D., Liu, C., 2022. A daily and 500 m coupled evapotranspiration and gross primary production product across China during 2000–2020. Earth Syst. Sci. Data 14, 5463–5488. https://doi.org/10.5194/essd-14-5463-2022

Hu, Z., Miao, Q., Shi, H., Feng, W., Hou, C., Yu, C., Mu, Y., 2023. Spatial Variations and Distribution Patterns of Soil Salinity at the Canal Scale in the Hetao Irrigation District. Water 15, 3342. https://doi.org/10.3390/w15193342

Jarvis, P.G., 1976. The interpretation of the variations in leaf water potential and stomatal conductance found in canopies in the field. Philosophical Transactions of the Royal Society of London. Series B, Biological Sciences 273, 593–610.

Katul, G., Manzoni, S., Palmroth, S., Oren, R., 2010. A stomatal optimization theory to describe the effects of atmospheric CO2 on leaf photosynthesis and transpiration. Annals of Botany 105, 431–442. https://doi.org/10.1093/aob/mcp292

Koenker, R., 2005. Quantile Regression. Cambridge University Press, Cambridge. https://doi.org/10.1017/CBO9780511754098

Li, C., Zhang, D., Zhang, S., Wen, Y., Wang, W., Chen, Y., Peng, J., 2025. Atmospheric Vapor Pressure Deficit Outweighs Soil Moisture Deficit in Controlling Global Ecosystem Water Use Efficiency. JGR Biogeosciences 130, e2024JG008605. https://doi.org/10.1029/2024JG008605

Li, X., Xiao, J., 2019. Mapping Photosynthesis Solely from Solar-Induced Chlorophyll Fluorescence: A Global, Fine-Resolution Dataset of Gross Primary Production Derived from OCO-2. Remote Sensing 11, 2563. https://doi.org/10.3390/rs11212563

Liu, L., Gudmundsson, L., Hauser, M., Qin, D., Li, S., Seneviratne, S.I., 2020. Soil moisture dominates dryness stress on ecosystem production globally. Nat Commun 11, 4892. https://doi.org/10.1038/s41467-020-18631-1

Medlyn, B.E., DUURSMA, R.A., EAMUS, D., ELLSWORTH, D.S., PRENTICE, I.C., BARTON, C.V.M., CROUS, K.Y., DE ANGELIS, P., FREEMAN, M., WINGATE, L., 2011. Reconciling the optimal and empirical approaches to modelling stomatal conductance. Global Change Biology 17, 2134–2144. https://doi.org/https://doi.org/10.1111/j.1365-2486.2010.02375.x

Monteith, J.L., 1965. Evaporation and Environment. Symposia of the Society for Experimental Biology 19, 205–34.

Munns, R., Tester, M., 2008. Mechanisms of salinity tolerance. Annual Review of Plant Biology 59, 651–681. https://doi.org/10.1146/annurev.arplant.59.032607.092911

Muñoz-Sabater, J., Dutra, E., Agustí-Panareda, A., Albergel, C., Arduini, G., Balsamo, G., Boussetta, S., Choulga, M., Harrigan, S., Hersbach, H., Martens, B., Miralles, D.G., Piles, M., Rodríguez-Fernández, N.J., Zsoter, E., Buontempo, C., Thépaut, J.-N., 2021. ERA5-Land: a state-of-the-art global reanalysis dataset for land applications. Earth Syst. Sci. Data 13, 4349–4383. https://doi.org/10.5194/essd-13-4349-2021

Novick, K.A., Ficklin, D.L., Grossiord, C., Konings, A.G., Martínez-Vilalta, J., Sadok, W., Trugman, A.T., Williams, A.P., Wright, A.J., Abatzoglou, J.T., Dannenberg, M.P., Gentine, P., Guan, K., Johnston, M.R., Lowman, L.E.L., Moore, D.J.P., McDowell, N.G., 2024. The impacts of rising vapour pressure deficit in natural and managed ecosystems. Plant, Cell & Environment 47, 3561–3589. https://doi.org/10.1111/pce.14846

Novick, K.A., Ficklin, D.L., Stoy, P.C., Williams, C.A., Bohrer, G., Oishi, A.C., Papuga, S.A., Blanken, P.D., Noormets, A., Sulman, B.N., Scott, R.L., Wang, L., Phillips, R.P., 2016. The increasing

importance of atmospheric demand for ecosystem water and carbon fluxes. Nature Clim Change 6, 1023–1027. https://doi.org/10.1038/nclimate3114

Oren, R., Sperry, J.S., Katul, G.G., Pataki, D.E., Ewers, B.E., Phillips, N., Schäfer, K.V.R., 1999. Survey and synthesis of intra- and interspecific variation in stomatal sensitivity to vapour pressure deficit. Plant, Cell & Environment 22, 1515–1526. https://doi.org/https://doi.org/10.1046/j.1365-3040.1999.00513.x

Ramos, T.B., Liu, M., Paredes, P., Shi, H., Feng, Z., Lei, H., Pereira, L.S., 2023. Salts dynamics in maize irrigation in the Hetao plateau using static water table lysimeters and HYDRUS-1D with focus on the autumn leaching irrigation. Agricultural Water Management 283, 108306. https://doi.org/10.1016/j.agwat.2023.108306

Sperry, J.S., Hacke, U.G., Oren, R., Comstock, J.P., 2002. Water deficits and hydraulic limits to leaf water supply. Plant, Cell & Environment 25, 251–263. https://doi.org/https://doi.org/10.1046/j.0016-8025.2001.00799.x

Wang, T., Zhang, J., Li, Z., Lin, K., Zhou, W., Wu, G., Pan, M., Chen, X., 2025. Roles of Soil and Atmospheric Dryness on Terrestrial Vegetation Productivity in China - Which Dominates at What Thresholds. Earth's Future 13, e2024EF005469. https://doi.org/https://doi.org/10.1029/2024EF005469

Wood, S.N., 2017. Generalized Additive Models: An Introduction with R, 2nd ed. Chapman and Hall/CRC. https://doi.org/10.1201/9781315370279

Xu, Z., Zhang, Y., Kong, D., Ma, N., Zhang, X., 2026. Extended global terrestrial evapotranspiration and gross primary production dataset from 1982 to near present. Earth System Science Data Discussions [discussion paper, under review]. https://doi.org/10.5194/essd-2026-94

Yu, R., Liu, T., Xu, Y., Zhu, C., Zhang, Q., Qu, Z., Liu, X., Li, C., 2010. Analysis of salinization dynamics by remote sensing in Hetao Irrigation District of North China. Agricultural Water Management 97, 1952–1960. https://doi.org/10.1016/j.agwat.2010.03.009

Zhang, Q., Ficklin, D.L., Manzoni, S., Wang, L., Way, D., Phillips, R.P., Novick, K.A., 2019. Response of ecosystem intrinsic water use efficiency and gross primary productivity to rising vapor pressure deficit. Environ. Res. Lett. 14, 074023. https://doi.org/10.1088/1748-9326/ab2603

Zhang, Q., Manzoni, S., Katul, G., Porporato, A., Yang, D., 2014. The hysteretic evapotranspiration—Vapor pressure deficit relation. JGR Biogeosciences 119, 125–140. https://doi.org/10.1002/2013JG002484

Zhang, Y., Kong, D., Gan, R., Chiew, F.H.S., McVicar, T.R., Zhang, Q., Yang, Y., 2019. Coupled estimation of 500 m and 8-day resolution global evapotranspiration and gross primary production in 2002–2017. Remote Sensing of Environment 222, 165–182. https://doi.org/10.1016/j.rse.2018.12.031

Supplementary Files

This is a list of supplementary files associated with this preprint. Click to download.

- SupplementaryFiguresS1S3.docx